PCCP

Accepted Manuscript

ROYAL SOCIETY OF CHEMISTRY

www.rsc.org/pccp

Structures of Seven Molybdenum Surfaces and Their Coverage Dependent Hydrogen Adsorption

Tao Wang,[a] Xinxin Tian,[b] Yong Yang,[b,c] Yong-Wang Li,[b,c] Jianguo Wang,[b] Matthias Beller,[a] Haijun Jiao[a,b,*]

a) Leibniz-Institut für Katalyse e.V. an der Universität Rostock, Albert-Einstein Strasse 29a, 18059 Rostock, Germany; b) State Key Laboratory of Coal Conversion, Institute of Coal Chemistry, Chinese Academy of Sciences, Taiyuan, Shanxi, 030001, PR China. c) National Energy Center for Coal to Liquids, Synfuels China Co., Ltd, Huairou District, Beijing, 101400, China.

E-mail address: haijun.jiao@catalysis.de

Abstract

Systematic density functional theory calculations and *ab initio* atomistic thermodynamics were applied to investigate the stability of seven metallic Mo surfaces [(110), (211), (111), (321), (310), (210) (100)] and their coverage dependent hydrogen adsorption. Only dissociative hydrogen adsorption is favored on these surfaces up to more than one monolayer saturation coverage. The computed hydrogen desorption temperatures on Mo(100) at 500 K and on Mo(110) at 410 K are in agreement with the available temperature-programmed desorption results. Under the consideration of H_2 as reduction reagent in Mo catalyst preparation, the computed surface morphology of Mo single crystal shows only exposed (110), (211) and (100) at high temperature; and the estimated surface proportion order of (110) > (211) > (100) agrees very well with the X-ray diffraction detected intensity order of (110) > (211) > (100). Surface reconstruction upon hydrogen adsorption has also been discussed.

Keywords: Hydrogen, Adsorption, Molybdenum, Morphology, Coverage, DFT

1. Introduction

Interactions of hydrogen with transition metals are simple but very essential in many industrial processes, such as Fischer-Tropsch synthesis,[1,2] ammonia synthesis,[3] water-gas shift reaction,[4] and hydro-treating reactions.[5] Hydrogen-metal systems are often used in characterizing the structures of solid surfaces and exploring the hydro-treating activity or the hydrogen-storing ability of metals. Among these transition metals, molybdenum is attractive, because it is the parent metal of many promising heterogeneous catalysts such as molybdenum carbide (Mo_2C),[6,7] molybdenum sulfide (MoS_2)[8] and molybdenum nitride.[9] Mo has been used as promoter in iron-based FTS catalysts to increase the tolerances of carbon deposition and sulfur.[10-12] Thus, investigating the catalytic property of metallic Mo is interesting and necessary from the aspects of fundamental academic researches and industrial applications.

On the basis of the important hydrogen-metal interactions, early ultra-high vacuum (UHV) surface science studies were extensively performed to detect the surface structures of metal substrates and hydrogen adsorption. For example, Dooley III and Haas[13] investigated the change of the Mo(100) surface upon hydrogen adsorption at different coverage. Altman *et al*.,[14] studied the phase transformations of the H/Mo(110) surface and no surface reconstruction was found upon hydrogen adsorption. Han and Schmidt[15] studied hydrogen binding states on the Mo(100) surface and found three hydrogen desorption states. However, they did not identify the exact hydrogen adsorption configurations. Using low energy electron diffraction (LEED), thermal desorption spectroscopy (TDS) and high resolution electron energy loss spectroscopy (HREELS) techniques, Zaera *et al*.,[16] found coverage dependent hydrogen adsorption on the Mo(100) surface. On the basis of LEED and surface infrared (IR) spectroscopy, Prybyla *et al*.,[17] studied hydrogen adsorption on the Mo(100) surface and found hydrogen atoms in bridge adsorption configuration under all conditions. A combined *ab initio* and helium-atom-scattering study of H-covered Mo(110) surface did not show any evidence of surface reconstruction.[18] Apart from the studies of phase transformation and surface reconstruction of the Mo(110) surface, extensive LEED and HREELS investigations[19-21] revealed that hydrogen atoms prefers the quasi-trigonal site and a (1×1)-H phase was identified at saturation monolayer coverage. On the Mo(111) surface,[22] a combined DFT calculation and LEED study revealed that the bridge adsorption sites between the top two layers are most favored and there are three adatoms per surface unit cell at saturation coverage. In addition to the clean the Mo surface, Li *et al*.,[23] investigated the effect of potassium on hydrogen adsorption and found potassium induced hydrogen adsorption states. Kröger *et al*.,[24] compared the surface dynamics of the H/Mo(110) and Li/Mo(110) systems to explain the strong substrate surface phonon anomalies. Chuikov *et al*.,[25] considered the kinetic isotope effects of low-temperature hydrogen adsorption on the Mo(110) surface, and found significant effects of the quantum properties of H_2 and D_2.

Apart from these above-mentioned UHV surface science studies, there are relatively limited theoretical analysis of hydrogen interaction with Mo surfaces. On the basis of density functional theory (DFT) calculations, Yakovkin *et al*.,[26] found that hydrogen atoms occupy the three-fold sites for the whole coverage on the Mo(110) surface, and proposed a microscopic model for associative hydrogen desorption. Zhou *et al*.,[27] reported an DFT study of hydrogen adsorption on the Mo(110) surface, and found the hollow site being most stable at a wide range of coverage and the sub site hydrogen adsorption becoming possible at one monolayer coverage. Ferrin *et al*.,[28] calculated hydrogen adsorption and diffusion on and in the surfaces of seventeen transition metals, where the interactions of hydrogen with the Mo(100) and (110) surfaces were included.

To the best of our knowledge, theoretical investigations of hydrogen interaction with Mo catalyst are far from complete, and there is no clear-cut and systematic understanding of this simple and useful system. Our previous works about hydrogen interactions with iron[29] and carbide surfaces[30] have proved that our methods can not only reproduce the available UHV surface science results but also can be used to predict the properties of such complex surfaces beyond the scope of UHV experiments. Most importantly, our studies provided a systematic and clear understanding into the structural and energetic properties of such systems. To further

extend our methodology and to have a whole insight into the H/Mo system, we systematically calculated hydrogen adsorption on seven Mo surfaces at different coverage since H_2 dissociative adsorption on Mo surfaces was proved by early experimental studies.[31] Throughout our studies, the effects of temperature and hydrogen partial pressure were included and the influence of hydrogen on the morphologies of Mo catalyst was also considered.

2. Computational methods and models

2.1 Methods: All results were obtained by applying the plane-wave based density functional theory (DFT) method with the Vienna *Ab Initio* Simulation Package (VASP)[32,33] and periodic slab models. The electron ion interaction was described with the projector augmented wave (PAW) method,[34,35] while the electron exchange and correlation energy was solved within the generalized gradient approximation in the Perdew-Burke-Ernzerhof formalism (GGA-PBE).[36] An energy cut-off of 400 eV and a second-order Methfessel-Paxton[37] electron smearing with σ = 0.2 eV were used to ensure accurate energies with errors less than 1 meV per atom. Geometry optimization was done when forces became smaller than 0.02 eV/Å and energy difference was lower than 10^{-4} eV. The vacuum layer between periodically repeated slabs was set as 10 Å to avoid interactions among the slabs. Since there are no differences in energies and lattice parameters between results with and without spin polarization (Table S1), we did not include spin-polarization in our results. Zero-point energy was included throughout the calculations of hydrogen adsorption. Since we only considered hydrogen adsorption on one side of the slab and did not use the symmetric slabs, dipole corrections were included in all our calculations.

2.2 Models and surface stability: The calculated lattice constant of Mo bulk crystal structure (3.17 Å) agrees with the experiment (3.15 Å).[38] To understand the properties of Mo catalyst, we firstly investigated the stability of seven Mo surfaces; the low Miller index (100), (110) and (111) surfaces for the basic structures, and the high Miller index (210), (211), (310) and (321) surfaces for the kinked, stepped and terrace structures. Mo surface energy (γ) is defined as: $\gamma_{(hkl)} = [E_{Mo(hkl)} - nE_{(Mo\text{-}bulk)}]/2A$, where $E_{Mo(hkl)}$ is the total energy of chosen Mo surface, $E_{(Mo\text{-}bulk)}$ is the bulk energy of Mo metal and A is the area of the surface. On the basis of systematic test of slab thickness (Table S2), we finally estimated the stability order of (110) > (211) > (111) > (321) > (310) > (210) > (100) with the surface energy of 2.76, 2.89, 2.97, 3.01, 3.09, 3.11 and 3.17 J/m^{-2}, respectively, where (110) is most stable and (100) is least stable. On the basis of these surface energies, we further performed Wulff construction[39,40] to present the ideal morphology of Mo catalyst. Under ideal condition (**Fig. 1**), (110) (44.9%) and (211) (39.7%) are most exposed, followed by (310) (11.6%) , (111) (2.7%) and (100) (1.1%). No exposed (210) and (321) could be found.

(Fig. 1)

For hydrogen adsorption, we used the *p*(3×3)-4L/R2 (layers of slab/relaxed layers), *p*(3×3)-4L/R2, *p*(2×3)-6L/R3, *p*(3×2)-8L/R4, *p*(3×2)-6L/R3, *p*(3×2)-6L/R3 and *p*(2×3)-8L/R4 super cells for the (100), (110), (111), (210), (211), (310) and (321) surfaces, respectively. The 3×3×1 Monkhorst-Pack k-point grid was applied in all surfaces for sampling the Brillouin zone.

2.3 Thermodynamics: *Ab initio* atomistic thermodynamics is a convenient tool to solve problems referring to environmental conditions[41,42] and has been widely and successfully applied in many catalytic systems.[43-50] The detailed description of the method can be found in Supplementary Information. The chemical potentials of H_2 were calculated from Gaussian 09 software (BP86/6-311G), which are in good agreement with the results from NIST database (Table S3). For the vibration computations, we only calculated the vibrational frequencies of adsorbed H atoms and did not consider that of the slabs. This is because that compared to the large vibrational contribution of gaseous hydrogen molecules, the contribution of solid surfaces is negligible for their large mass differences.

3 Results and discussions

3.1. Surface structures and adsorption sites: As shown in **Fig. 2**, each surface has characteristic structure for hydrogen adsorption. For example, (100) has one top (**T**), one bridge (**B**) and one 4-fold hollow (**4F**) sites; (110) has one top (**T**), one short-bridge (**SB**), one

long-bridge (**LB**) and one 3-fold (**3F**) sites; (111) has one top (**T**), three bridge (**B_1-B_3**), one shallow-hollow (**SH**), one deep-hollow (**DH**) and one 4-fold hollow (**4F**) sites; (210) has three top (**T_1**, **T_2**, **T_3**), three bridge (**B_1**, **B_2**, **B_3**), four 3-fold (**$3F_1$**, **$3F_2$**, **$3F_3$**, **$3F_4$**) and one 4-fold (**4F**) sites; (211) has one top (**T**), one bridge (**B**), two 3-fold (**$3F_1$**, **$3F_2$**) and one 4-fold (**4F**) sites; (310) has one top (**T**), one bridge site (**B**), two 3-fold (**$3F_1$**, **$3F_2$**) and one 4-fold (**4F**) sites, while (321) has three top (**T_1**, **T_2**, **T_3**), two bridge (**B_1**, **B_2**), six 3-fold (**$3F_1$**, **$3F_2$**, **$3F_3$**, **$3F_4$**, **$3F_5$**, **$3F_6$**) and one 4-fold (**4F**) sites. On the basis of these distinct surface structures and adsorption sites, different hydrogen adsorption properties can be expected.

(Fig. 2)

3.2. Hydrogen adsorption at different coverage: To discuss the adsorption of specific species on solid surfaces, coverage effect is important and has intimated relationships with surface structure and reaction conditions. Thus, we firstly systematically identified the stable adsorption structures of H atoms at different coverage, where the stepwise adsorption energy ($\Delta E_{ads} = E_{(H)n+1/slab} - [E_{(H)n/slab} + 1/2E_{H2}]$) is used to determine the saturation coverage. It should be noted that during the identification of the most stable configurations at different coverage, we firstly tested all possible structures by adding one more H atom on the previously most stable coverage on the basis of the individual adsorption energies at different adsorption sites. In addition, we also tested other different arrangements of those N atoms at the corresponding coverage. Our goal is to find the most stable one by considering as many as different possibilities. Finally, a positive ΔE_{ads} for n+1 adsorbed H atoms indicates the saturation adsorption with nH atoms.

On Mo(100) at the lowest coverage (**Fig. S1**), the adsorbed H atom is located at the bridge site with adsorption energy of -1.10 eV. With the increase of hydrogen coverage, the stepwise adsorption energy gradually decreases, but the bridge site is always most favored. The saturation monolayer coverage has 18H atoms at the bridge sites (**Fig. 3**). Further inspection revealed weak deformation of some surface Mo atoms from their original positions at low hydrogen coverage ($n_H < 8$). However, such deformation disappears at hydrogen coverage higher than 8H. All these findings are in perfect agreement with the available UHV study by Prybyla *et al*.,[17] i.e.; all H atoms are located at the bridge sites at all coverage and temperatures, and the surface is reconstructed at low coverage and slowly relaxes back to its bulk value with increasing coverage. This agreement gives us the confidence to apply our models and methods to further explore the interaction mechanisms of hydrogen on the other Mo surfaces.

On Mo(110) at the lowest coverage (**Fig. S2**), the adsorbed H atom is located at the **3F** site (-0.70 eV). With the increase of hydrogen coverage, the adsorbed H atoms are still located at the **3F** sites, and this is in line with the previous experimental[19-21] and DFT[26-28] results. At the saturation monolayer coverage (**Fig. 3**), there are 9H atoms on the p(3×3) surface, which corresponds to a c(1×1)-H phase. This optimized structure at saturation monolayer coverage is in agreement with the available LEED results from UHV experiments.[19-21] The stepwise adsorption energies of these H atoms are very close up to saturation, indicating their negligible repulsive interactions. In addition, no surface reconstructions upon hydrogen adsorption could be found.

On Mo(111) at the lowest coverage (**Fig**. **S3**), the adsorbed H atom is located at the **B_1** site between the first and second layer Mo atoms (-0.71 eV). With nH = 1-6, all H atoms are still located at the **B_1** sites and the stepwise adsorption energies are very close, indicating their negligible repulsive interactions. With the increase of hydrogen coverage, the value of ΔE_{ads} decreased regularly and the saturation coverage was reached at nH = 20 (**Fig. 3**). At the saturation coverage, all H atoms are located at the **B_1** sites and each surface unit cell has almost three H atoms, and these findings are in line with the early UHV study.[22]

On Mo(210) at the lowest coverage (**Fig. S4**), the adsorbed H atom is located at the **$3F_2$** hollow site (-0.79 eV). With the increase of hydrogen coverage, different adsorption configurations became possible and the saturation coverage was found at nH = 30 (**Fig. 3**), where the top, bridge, 3F hollow as well as 4F hollow adsorption configurations are found on the surface.

On Mo(211) at the lowest coverage (**Fig. S5**), the adsorbed H atom is located at the **B_1** site (-0.93 eV) and the saturation coverage

has 12H atoms (**Fig. 3**), and all the H atoms are located on the $\mathbf{B_1}$ sites.

On Mo(310) at the lowest coverage (**Fig. S6**), the adsorbed H atom is located on the $\mathbf{3F_1}$ hollow site (-0.78 eV). With the increase of hydrogen coverage, different adsorption configurations became possible and the saturation coverage has 18H atoms (**Fig. 3**) with **B**, **3F1** and **4F** adsorption configurations coexisting.

On Mo(321) at the lowest coverage (**Fig. S7**), the adsorbed H atom is located on the bridge site (-0.78 eV). However, the **3F** hollow site became favored with the increase of hydrogen coverage and finally the saturation coverage has 18H atoms (**Fig. 3**), and all H atoms are located at the **3F** sits.

(Fig. 3)

At the lowest coverage, the adsorption energy of one H atom follows the order of the surface stability, i.e.; the least stable Mo(100) surface has the strongest adsorption energy and the most stable Mo(110) surface has the weakest adsorption energy. At the saturation coverage (**Fig. 3**), the high miller index surfaces have much higher coverage than the low miller index surfaces, i.e.; the Mo(210) surface has a saturation coverage of 5 monolayer H atoms, which indicates its high ability in storing hydrogen. To discuss the effects of hydrogen adsorption on electronic structures of Mo surfaces, we performed Bader charge analysis on each surface at different hydrogen coverage. It is found that Mo surfaces donate electrons to the adsorbed hydrogen atoms and the amounts of donated electrons increased with increasing hydrogen coverage (Table S4), and this is because that a H atom is more electronegative than a Mo atom on the basis of the Allen electronegativity scale (2.30 and 1.47, respectively).[51]

3.3. Stable hydrogen coverage with T and p_{H2}: In the above part, we identified the stable hydrogen adsorption configurations at different coverage and provided the detailed energetic and structural information from standard DFT calculations under ideal condition. Since those results cannot represent hydrogen adsorption properties on Mo catalyst under practical conditions, we introduced the effects of temperature and hydrogen pressure into our systems and used the adsorption Gibbs free energy as the criteria for discussion. On the basis of *ab initio* atomistic thermodynamics, we built the phase diagrams of hydrogen adsorption on each Mo surface, which present the relationship between the stable H coverage with temperatures as well as hydrogen partial pressure.

As shown in **Fig. 4**, each phase diagram has several regions representing different stable hydrogen coverage at given conditions, e.g.; the stable hydrogen coverage decreases with increasing temperature at given pressures, while increases with H_2 partial pressure at given temperature. On the basis of these equilibrium phase diagrams, one can easily estimate the stable hydrogen coverage at any given T and p_{H2}. Close inspections also revealed that the stable hydrogen coverage on these seven Mo surfaces is different from each other under the same conditions, indicating their quite different hydro-treating activities.

(Fig. 4)

These phase diagrams can also provide some references for UHV surface science studies, micro-kinetics modeling and practical experimental applications. Among these advantages, estimating hydrogen desorption temperatures is highly related to temperature programmed desorption (TPD) from UHV surface science studies. Normally, TPD was performed under UHV condition with a base pressure of about 1×10^{-10} Torr (10^{-13} atm). We therefore chose $\ln(p_{H2}/p^0) = -28$ as an example to estimate hydrogen desorption temperatures on each surface, which is also a UHV pressure. On the basis of the phase diagrams in **Fig. 4**, we can easily get the temperatures for full hydrogen desorption. For instance, the full hydrogen desorption temperature is about 500, 410, 400, 475, 500, 450 and 480 K on the (100), (110), (111), (210), (211), (310) and (321) surfaces, respectively (**Table 2**). Actually, our estimated full hydrogen desorption temperatures on the Mo(100) and (110) surfaces are in good agreement with the available experiment H_2-TPD/Mo results. For example, Zaera *et al.*,[16] found that all the H-Mo frequency signals disappear on the Mo(100) surface at temperature higher than 500 K, which is the same as our estimated full hydrogen desorption temperature. Mahnig and Schmidt[52] found that the

desorption peak related to associative hydrogen desorption one the Mo(110) surface is observed at temperature about 400 K, which is also very similar to our theoretically predicted 410 K. All these agreements between theory and experiment validated our methodology and gave us the confidence for other systems.

(Table 2)

3.4. Wulff Particles of Mo catalyst: In practical, reduction of MoO_3 powders by hydrogen is one of the most used methods to obtain metallic molybdenum with high purity.[53] Therefore, hydrogen should play an essential role in determining the structure of metallic Mo catalyst. Generally, the activity of catalysts was always affected by their surface structures and compositions. Furthermore, the morphology of catalysts is highly related to the preparation conditions and environment. We therefore considered the effects of hydrogen on the surface stability and morphology of Mo catalyst. In this part, *ab initio* atomistic thermodynamics was applied to address the influences of hydrogen adsorption on the surface free energies. Briefly, each Mo surface should have different numbers of hydrogen under chosen condition, which will cause different changes in the corresponding surface energy. As shown in **Table 1**, we presented the surface free energies of each surface at different temperatures and p_{H2} = 1 atm. It clearly revealed that hydrogen adsorption lowered the surface free energies and affected the surface stabilities. On the basis of the surface free energies of each surface, Wulff construction was performed to reveal the morphologies of Mo catalyst at different conditions.

At p_{H2} = 1 atm, four temperatures at 0, 425, 675 and 775 K, were chosen (**Fig. 5**). At 0 K and p_{H2} = 1 atm, the most exposed surface is Mo(100), followed by (211), (321), (210) and (110). With the increase of temperature, the proportion of Mo(100) decreases while those of Mo(110) and (211) increase. At 775K and p_{H2} = 1 atm, only Mo(100), (110) and (211) are exposed, where (110) is most exposed, followed by (211) and (100). Interestingly, this result is in very good agreement with available experimental result by Qian and Lim,[54] where the X-ray diffraction (XRD) result gave an intensity order of Mo(110) > Mo(211) > Mo(100) for the prepared metallic Mo catalyst. This good agreement between theory and experiment further strongly verified our applied methods and models, and this methodology should play a very essential complementary role for further UHV surface science studies for such systems.

(Fig. 5)

4. Conclusion

Density functional theory calculation and atomistic thermodynamics were applied to investigate the surface stability of the (100), (110), (111), (210), (211), (310) and (321) surfaces of Mo as well as their hydrogen adsorption properties at given temperature and pressure. On the basis of the computed surface free energies at ideal condition, the surface stability follows the order of (110) > (211) > (111) > (321) > (310) > (210) > (100), where (110) is most stable and (100) is least stable.

On all these surfaces, only dissociative hydrogenation is found and this is in agreement with the available experimental studies. It is also found that these surfaces can have more than one monolayer saturation coverage, especially on the high index surfaces. Under the consideration of temperature and pressure, the coverage effect has been discussed, and particularly, the hydrogen desorption temperatures on the surfaces under the UHV condition have been computed. It is interestingly noted that the computed hydrogen desorption temperatures on Mo(100) at 500K and on Mo(110) at 410 K agree perfectly with the detected values from the temperature-programmed desorption studies at 500 and 400 K, respectively.

In addition we also computed the surface morphology of Mo single crystal under the consideration of H_2 as reduction reagent in the preparation process. It is found that the surface morphology depends on temperature. At high temperature and one atmosphere of hydrogen pressure, only the (110), (211) and (100) surfaces are exposed and the estimated surface proportion ratio is in perfect agreement with the XRD detected intensity order of (110) > (211) > (100).

All these agreements between theory and experiments nicely validated our methodology, which can be straightforwardly used to other systems.

Acknowledgment: This work was supported by National Natural Science Foundation of China (No. 21273262), National Basic Research Program of China (No. 2011CB201406), Chinese Academy of Sciences and Synfuels CHINA. Co., Ltd. We also acknowledge general finical support from the BMBF and the state of Mecklenburg-Western Pommerania.

Electronic Supplementary Information (ESI) available: Detailed description of atomistic thermodynamics method; effects of spin polarization (Table S1); slab thickness tests for surface energy calculations (Table S2); hydrogen chemical potential (Table S3), Bader charges of Mo surfaces (Table S4) as well as structures and energies of H atoms adsorption on seven Mo surfaces (Fig. S1-S7) are included.

Table 1: Surface energies (J/m^{-2}) of seven Mo surfaces under ideal and hydrogen atmosphere (p_{H2} = 1 atm)

Surface	ideal	0K/H_2	425K/H_2	675K/H_2	775K/H_2
Mo(110)	2.76	1.50	2.06	2.49	2.26
Mo(211)	2.89	1.41	2.05	2.54	2.41
Mo(111)	2.97	1.58	2.28	2.78	2.75
Mo(321)	3.01	1.45	2.08	2.55	2.54
Mo(310)	3.09	1.65	2.34	2.78	2.85
Mo(210)	3.11	1.43	2.22	2.65	2.77
Mo(100)	3.17	1.18	1.96	2.58	2.83

Table 2: Full desorption temperatures of hydrogen on each surface at $\ln(p_{H2}/p^0) = -28$.

Surface	Theory	Experiment
(110)	500 K	500 K[16]
(100)	410 K	400 K[52]
(111)	400 K	-
(211)	475 K	-
(210)	500 K	-
(310)	450 K	-
(321)	480 K	-

Fig. 1: Ideal Wulff particle of metallic molybdenum

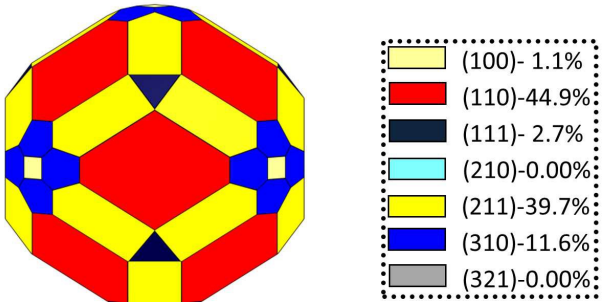

Fig. 2: Schematic top and side views of seven Molybdenum surfaces and possible adsorption sites (T for top, B for bridge, F for fold, LB for long bridge, SB for short bridge, SH for shallow hollow and DH for deep hollow)

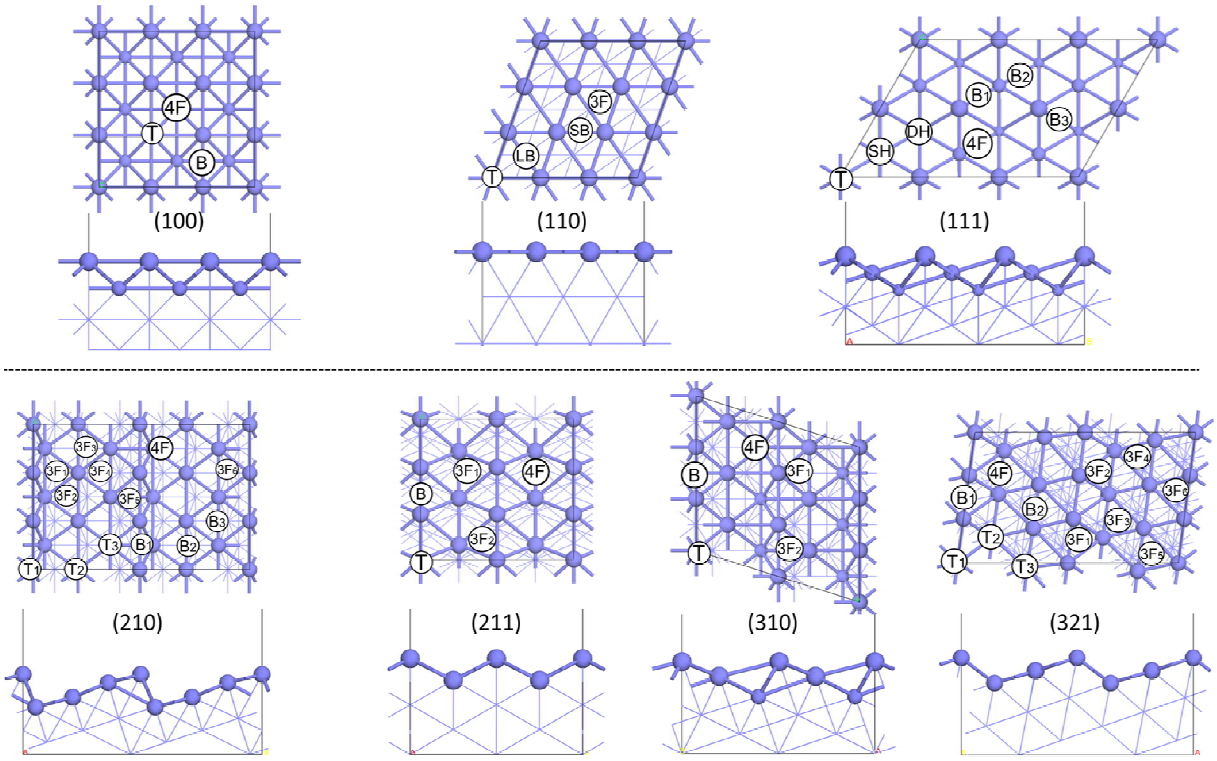

Fig. 3: Adsorption structures of hydrogen at saturation coverage on seven Mo surfaces

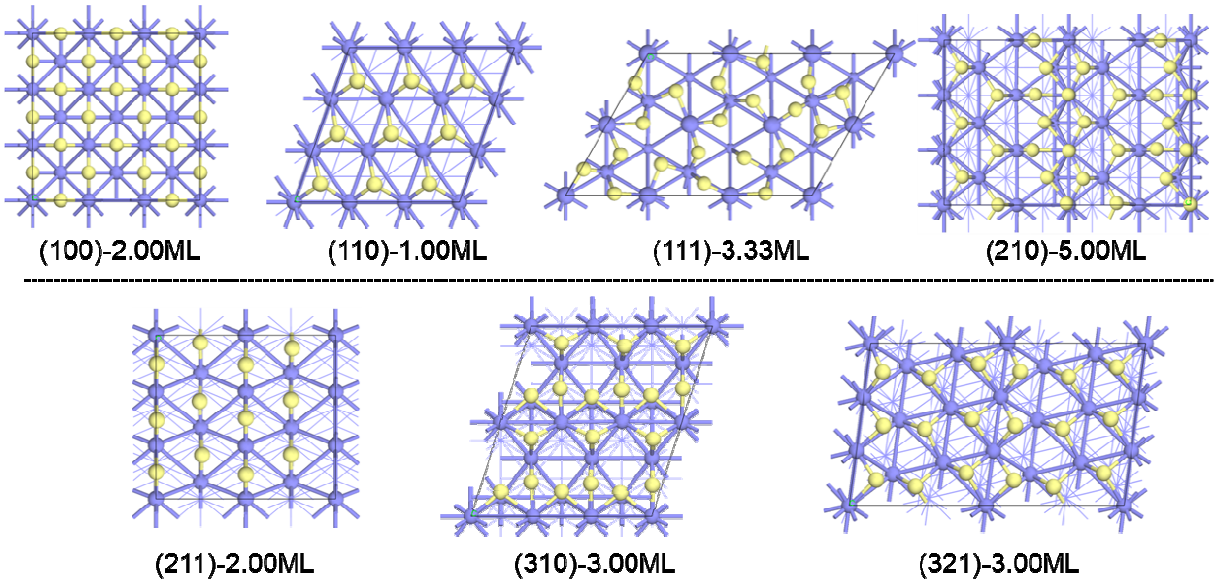

Fig. 4: Phase diagrams of stable hydrogen coverage at different conditions

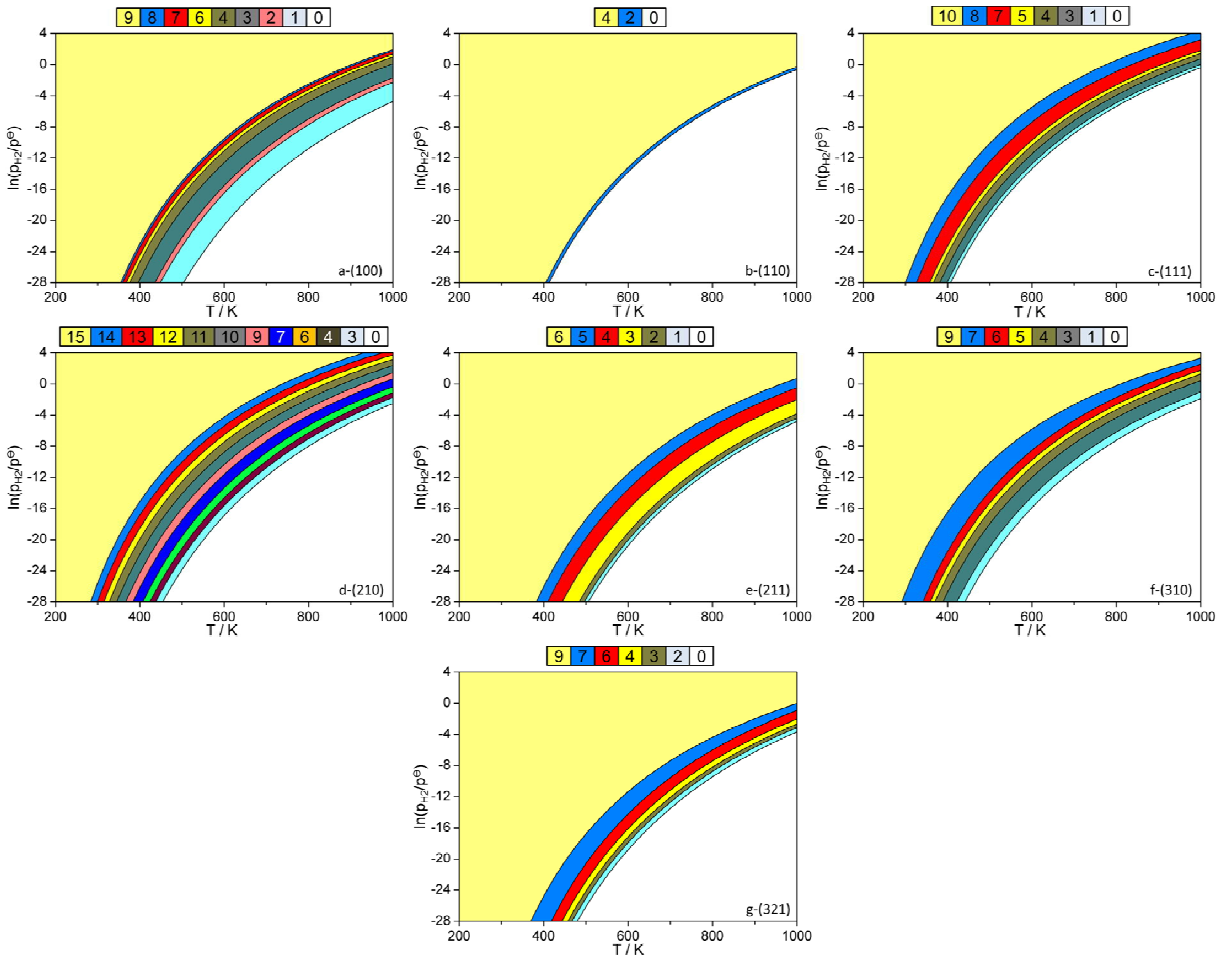

Fig. 5: Morphologies of metal Mo catalyst under different hydrogen pretreatment conditions

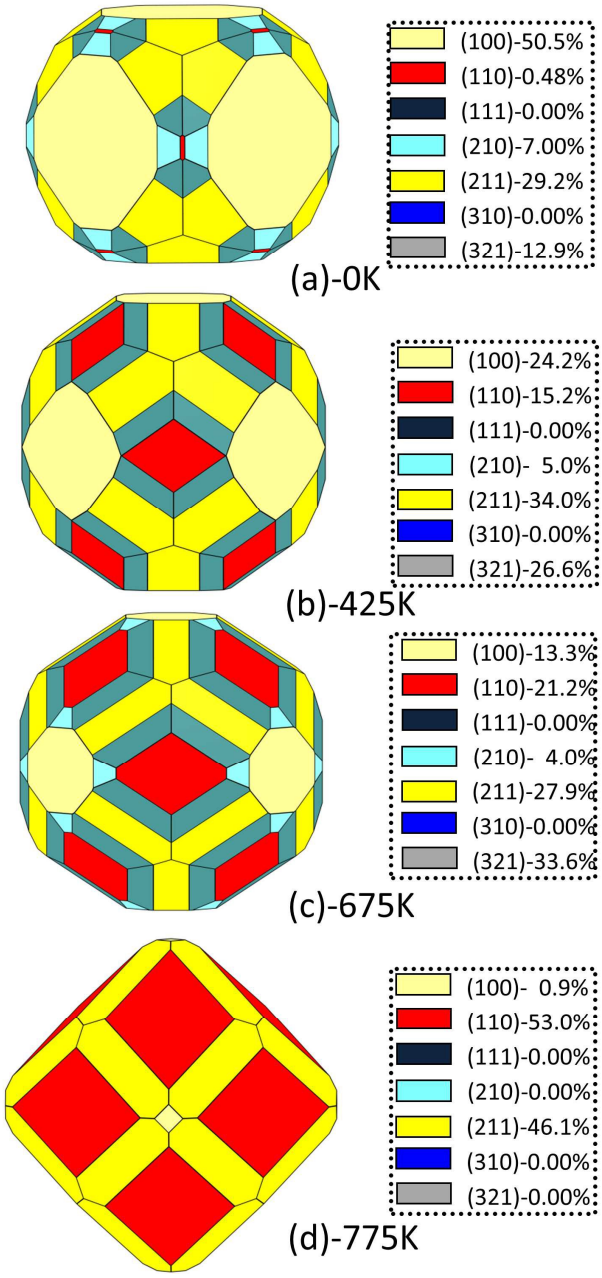

Reference

1 E. de Smit and B. M. Weckhuysen, *Chem. Soc. Rev*. 2008, **37**, 2758-2781.

2 P. C. Thüne, C. J. Weststrate, P. Moodley, A. M. Saib, J. van de Loosdrecht, J. T. Miller and J. W. Niemantsverdriet, *Catal. Sci. Technol*. 2011, **1**, 689-697.

3 G. Ertl, *Angew. Chem. Int. Ed*. 2008, **47**, 3524-3535.

4 D. S. Newsome, *Cat. Rev. - Sci. Eng*. 1980, **21**, 275-318.

5 H. Topsøe, B. S. Clausen and F. E. Massoth, Springer-Verlag: Berlin, 1996.

6 J. G. Chen, *Chem. Rev.* 1996, **96**, 1447-1498.

7 H. H. Hwu and J. G. Chen, *Chem. Rev*. 2005, **105**, 185-212.

8 T. F. Jaramillo, K. P. Jørgensen, J. Bonde, J. H. Nielsen, S. Horch and I. Chorkendorff, *Science* 2007, **317**, 100-102.

9 S. Ramanathan and S. T. Oyama, *J. Phys. Chem*. 1995, **99**, 16365-16372.

10 S. D. Qin, C. H. Zhang, B. S. Wu, J. Xu, H. W. Xiang and Y.-W. Li, *Catal. Lett*. 2010, **139**, 123-128.

11 X. J. Cui, J. Xu, C. H. Zhang, Y. Yang, P. Gao, B. S. Wu and Y.-W. Li, *J. Catal*. 2011, **282**, 35-46.

12 R. M. Malek Abbaslou, J. Soltan and A. K. Dalai, *Fuel* 2011, **90**, 1139-1144.

13 G. J. Dooley and T. W. Haas, *J. Chem. Phys.* 1970, **52**, 993-996.

14 M. Altman, J. W. Chung, P. J. Estrup, J. M. Kosterlitz, J. Prybyla, D. Sahu and S. C. Ying, *J. Vac. Sci. Technol. A* 1987, **5**, 1045-1048.

15 H. R. Han and L. D. Schmidt, *J. Phys. Chem*. 1971, **75**, 227-234.

16 F. Zaera, E. B. Kollin and J. L. Gland, *Surf. Sci. Lett.* 1986, **166**, L149-L154.

17 J. A. Prybyla, P. J. Estrup and Y. J. Chabal, *J. Chem. Phys*. 1991, **94**, 6274-6295.

18 B. Kohler, P. Ruggerone and M. Scheffler, *Phys. Rev. B* 1997, **56**, 13503-13518.

19 J. Kröger, S. Lehwald and H. Ibach, *Phys. Rev. B* 1997, **55**, 10895-10904.

20 M. Okada, A. P. Baddorf and D. M. Zehner, *Surf. Sci*. 1997, **373**, 145-152.

21 J. Kröger, S. Lehwald and H. Ibach, *Surf. Sci*. 1998, **402**, 496-501.

22 M. Arnold, A. Fahmi, W. Frie, L. Hammer and K. Heinz, *J. Phys.: Condens. Matter* 1999, **11**, 1873-1888.

23 Z. Y. Li, E. M. Mccash and W. Allison, *Surf. Sci*. 1991, **251**, 905-910.

24 J. Kröger, S. Lehwald and H. Ibach, *Surf. Sci*. 2003, **530**, 170-174.

25 B. A. Chuikov, V. D. Osovskii, Y. G. Ptushinskii and V. G. Sukretnyi, *Surf. Sci*. 2000, **448**, L201-L206.

26 I. N. Yakovkin, V. D. Osovskii, N. V. Petrova and Y. G. Ptushinsk, *Surf. Rev. Lett*. 2006, **13**, 375-386.

27 Y. G. Zhou, X. T. Zu, J. L. Nie and H. Y. Xiao, *Chem. Phys*. 2008, **351**, 19-26.

28 P. Ferrin, S. Kandoi, A. U. Nilekar and M. Mavrikakis, *Surf. Sci*. 2012, **606**, 679-689.

29 T. Wang, S. G. Wang, Q. Q. Luo, Y.-W. Li, J. Wang, M. Beller and H. Jiao, *J. Phys. Chem. C* 2014, **118**, 4181-4188.

30 T. Wang, Y.-W. Li, J. Wang, M. Beller and H. Jiao, *J. Phys. Chem. C* 2014, **118**, 8079-8089.

31 B. A. Chuikov, V. D. Osovskii, Y. G. Ptushinskii and V. G. Sukretnyi, *Surf. Sci*. 2001, **473**, 143-150.

32 G. Kresse and J. Furthmüller, *Comput. Mater. Sci.* 1996, **6**, 15-50.

33 G. Kresse and J. Furthmüller, *Phys. Rev. B* 1996, **54**, 11169-11186.

34 P. E. Blochl, *Phys. Rev. B* 1994, **50**, 17953-17979.

35 G. Kresse, *Phys. Rev. B* 1999, **59**, 1758-1775.

36 J. P. Perdew, K. Burke and M. Ernzerhof, *Phys. Rev. Lett.* 1996, **77**, 3865-3868.

37 M. Methfessel and A. T. Paxton, *Phys. Rev. B* 1989, **40**, 3616-3621.

38 C. Kittel, *Introduction to Solid State Physics*, Wiley, New York, 1996.

39 http://www.ctcms.nist.gov/wulffman/.

40 http://www.geomview.org/.

41 K. Reuter and M. Scheffler, *Phys. Rev. B* 2001, **65**, 035406.

42 K. Reuter and M. Scheffler, *Phys. Rev. B* 2003, **68**, 045407.

43 W. X. Li, C. Stampfl and M. Scheffler, *Phys. Rev .B* 2003, **68**, 165412.

44 M. E. Grillo, W. Ranke and M. W. Finnis, *Phys. Rev .B* 2008, **77**, 075407.

45 F. Zasada, W. Piskorz, S. Cristol, J. F. Paul, A. Kotarba and Z. Sojka, *J. Phys. Chem. C* 2010, **114**, 22245-22253.

46 T. Wang, X. W. Liu, S. G. Wang, C. F. Huo, Y.-W. Li, J. Wang and H. Jiao, *J. Phys. Chem. C* 2011, **115**, 22360-22368.

47 T. Wang, S. G. Wang, Y.-W. Li, J. Wang and H. Jiao, *J. Phys. Chem. C* 2012, **116**, 6340-6348.

48 T. Wang, Y.-W. Li, J. Wang, M. Beller and H. Jiao, *J. Phys. Chem. C* 2014, **118**, 3162-3171.

49 T. Wang, X. Tian, Y.-W. Li, J. Wang, M. Beller and H. Jiao, *J. Phys. Chem. C* 2014, **118**, 1095-1101.

50 T. Wang, X. Tian, Y.-W. Li, J. Wang, M. Beller and H. Jiao, *ACS Catal.* 2014, **4**, 1991-2005.

51 L. C. Allen *J. Am. Chem. Soc*. 1989, **111**, 9003-9014.

52 M. Mahnig and L. D. Schmidt, *Z. F. Phys. Chem*. 1972, **80**, 71-81.

53 G. P. Martins, T. Kangsadan, G. Scott, C. Wagner and J. Van Hoose, *Mater Sci Forum* 2007, **561–565**, 447–452.

54 M. Qian and L. C. Lim, *J. Mater. Sci. Lett*. 1999, **18**, 1253-1254.

TOC